

Water-to-air transfer of nano/micro-sized particulates: enrichment effect in bubble bursting jet drops

Bingqiang Ji,^{†,¶} Amrit Singh,^{†,¶} and Jie Feng^{*,†,‡}

[†]*Mechanical Science and Engineering, University of Illinois at Urbana-Champaign, Urbana,
IL 61801, USA*

[‡]*Materials Research Laboratory, University of Illinois at Urbana-Champaign, Urbana, IL
61801, USA*

[¶]*These two authors contributed equally.*

E-mail: jiefeng@illinois.edu

Abstract

Bubbles dispersed in liquids are widely present in many natural and industrial processes, and play a key role in mediating mass transfer during their lifetime from formation to rising to bursting. In particular, nano/micro-sized particulates and organisms, present in the bulk water can be highly enriched in the jet drops ejected during bubble bursting, impacting global climate and public health. However, the detailed mechanism of this enrichment remains obscure, with the enrichment factor being difficult to predict. Here, we experimentally investigate the enrichment of nano/micro-sized particles in bubble bursting jet drops and highlight the underlying hydrodynamic mechanism, combining the effects of bubble scavenge and bursting on the transport of particles. Scaling laws for the enrichment factor are subsequently proposed that de-

scribe both our and prior experimental results reasonably well. Our study may provide new insights for water-to-air transfer of microbes related to bubble bursting.

Keywords

Nano/micro-sized particle, enrichment, bubble bursting, jet drop, disease transmission

Introduction

Bursting of bubbles at liquid surfaces is a ubiquitous process which generates film drops by cap disintegration and jet drops by the fragmentation of the upward liquid jet induced by cavity collapse.¹⁻⁴ In natural water bodies, bubbles are typically smaller than a millimeter in diameter,⁵⁻⁸ and mainly produce jet drops with a typical size of several to dozens of microns instead of film drops.⁹⁻¹³ These small drops may remain suspended in the air, containing various compositions from the bulk water,¹⁴ such as sea salts,^{3,15} surfactants,^{16,17} oil spills,^{18,19} nanoplastic and microplastic particles,^{20,21} and even nano/micro-sized organisms.²²⁻²⁴ Therefore, bubble bursting jets play an important role in mediating mass transfer across the air-water interface in a wide range of industrial, geological, and biological phenomena, including the flavor release from sparkling beverages²⁵, sea spray aerosol generation,^{3,13,26} oceanic vegetative reproduction,²⁷ and airborne pathogen transmission.^{28,29}

It has been widely recognized that both soluble and insoluble components can be substantially enriched in jet drops with a much higher concentration compared to that in the bulk water, up to a thousand fold.^{16,30-33} The enrichment of nano/micro-sized particles is of particular interest considering the transport of microbes by bursting bubbles in contaminated water,^{24,28} which may be one potential mechanism that increases the risk of airborne pathogen transmission.^{34,35} This enrichment is believed to be caused by the scavenging of suspended particles by the bubble during rising, and subsequently, the collection of the captured particles along with the liquid shell around the bubble cavity surface into the jet drops upon

bursting.^{30,32,36} A majority of the prior studies investigated bacteria enrichment by collecting the jet drops and then culturing the bacteria for measurement, with different bubble rising distances, bubble sizes, bacteria types and concentrations, as well as culture ages.^{28,37–43} However, due to the limitations of such an indirect measurement and the complexity of the biological systems, the enrichment factor of the bacteria reported by prior studies varied dramatically from 1 to 1000 even under the similar experimental conditions, and the detailed hydrodynamic mechanism is still elusive.⁴⁴ Therefore, predicting the enrichment factor of particulate matter in bubble bursting jet drops remains a formidable challenge.

Here, we experimentally investigate the enrichment of nano/micro-sized spherical particulates in bubble bursting jet drops in a controlled dispersal system by direct visualization of bubble dynamics and measurement of particulate concentrations. We provide the detailed hydrodynamic mechanism determining particle enrichment, and derive scaling laws which quantify the dependencies of particulate enrichment factor on the bubble and particle sizes, and the bubble rising distance. The proposed scaling laws quantitatively agree with our experimental results over a wide range of experimental parameters. Furthermore, for the first time, the scaling laws describe the main trend of the enrichment of bacteria in previous experiments, potentially advancing the framework for the modeling of water-to-air transmission of particulates involving bubble bursting jets.

Results and discussion

Particulate enrichment in top jet drops

In the experiments (Figure 1(A)), an air bubble of radius R_b is generated using a micropipette at a distance H beneath the surface of the aqueous suspension of fluorescent polystyrene (PS) particles with a number concentration of $C_b \approx 2.3 \times 10^6/\text{mL}$ (Figure 1(B), [Movie S1](#)). After rising to the water surface, the bubble rests and then bursts, ejecting jet drops upwards (Figure 1(C), [Movie S2](#)). We focus on the top jet drop ejected by the bursting bubble, which

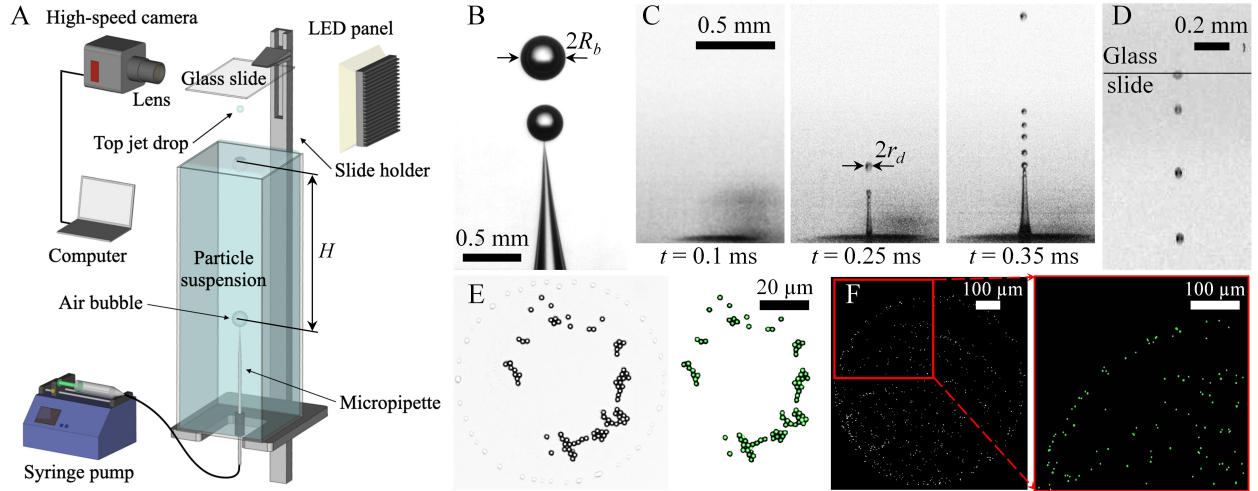


Figure 1: (A) Experimental setup. An air bubble is injected using a micropipette at a distance H beneath the surface of the aqueous particle suspension. After rising to the liquid surface, the bubble rests and then bursts, ejecting jet drops upwards. Only the top jet drop is collected by the glass slide. A high-speed camera is used to measure the bubble radius R_b and the top jet drop radius r_d . Experimental images show (B) a bubble of $R_b = 0.19$ mm forming and rising (Movie S1) before (C) bursting at the liquid surface and ejecting jet drops (Movie S2). Finally (D) the top jet drop of $r_d = 21 \mu\text{m}$ is collected by a glass slide (Movie S3). The images are superimposed every $\Delta t = 31.25$ ms and 0.2 ms for (B) and (D), respectively. (E) Original (left) and processed images with the particles identified by green dots (right) of the dried top jet drop, with $r_d = 34 \mu\text{m}$ and $r_p = 1 \mu\text{m}$. (F) Original (left) and processed (right) fluorescent images of a $0.33 \mu\text{L}$ drop of bulk particle suspension dried on the glass slide, with $r_p = 1 \mu\text{m}$.

has the highest enrichment as shown by previous studies.^{28,32,44} The formation and bursting of the bubble are visualized by a high-speed camera to measure R_b and the top jet drop radius r_d (See details in [Methods](#)). For a bubble bursting at a pure water surface, the top jet drop size is determined only by the Ohnesorge number ($Oh = \mu/\sqrt{\rho_w R_b \gamma}$ with μ , ρ_w , and γ representing the water viscosity, density, and surface tension, respectively, evaluating the effects of viscosity to inertial and surface tension) when the Bond number ($Bo = \rho_w g R_b^2/\gamma$ with gravitational acceleration g , evaluating the effects of gravity relative to surface tension) is negligible ($Bo < 0.16$ in our experiments).^{45–47} Figure 2(A) shows the dimensionless top jet drop radius r_d/R_b observed experimentally as a function of Oh , which is well described by the scaling law proposed by a previous study⁴⁸ on bubble bursting at a pure water surface,

$$\frac{r_d}{R_b} = 0.22(1 - (\frac{Oh}{0.031})^{0.5}), \quad (1)$$

indicating that the presence of the particles used in our experiments does not affect the jet dynamics of bubble bursting. In addition, the surface tensions of all the particle suspensions we used were confirmed to remain the same as that of water using the pendent drop method.

Only the top jet drop is collected using a glass slide placed above the water surface, verified by the high-speed camera (Figure 1(D), [Movie S3](#)). The particle numbers in the jet drop and bulk water, N_d and N_b , respectively, are quantified using microscope images of the collected dried jet drop (Figure 1(E)) and a dried bulk drop of volume V_b on a glass slide (Figure 1(F)), by either the bright field or fluorescent light. The enrichment factor (EF) of particulates in the top jet drop is calculated as

$$EF = \frac{N_d/V_d}{N_b/V_b} = \frac{3N_d}{4\pi r_d^3 C_b}. \quad (2)$$

We use nano/micro-sized spherical particles of $r_p = 0.25, 0.5$, and $1 \mu\text{m}$ as a representative model for viruses and bacteria based on size, with $R_b = 0.19 - 1.09 \text{ mm}$ and $H = 5 - 200 \text{ mm}$. As shown in Figures 2(B) and 2(C), we observe an EF varied between 6 and 571,

which is consistent with that reported by previous studies.^{30,32} Specifically, EF increases with the bubble rising distance H in approximate linearity since more particles may be captured by the rising bubble with a larger H . In addition, EF increases significantly with decreasing bubble radius R_b , which is approximately 571 and 18 when $R_b = 0.19$ and 1.09 mm with $H = 200$ mm, respectively. Furthermore, we find that the particle radius r_p barely affects EF at a range of $r_p = 0.25 - 1 \mu\text{m}$. To rationalize the effects of different parameters on EF , we will further discuss the bubble hydrodynamics contributing to the particulate enrichment in the top jet drop, including the scavenging of particles during bubble rising, and the collection of particles into the jet drop upon bursting.

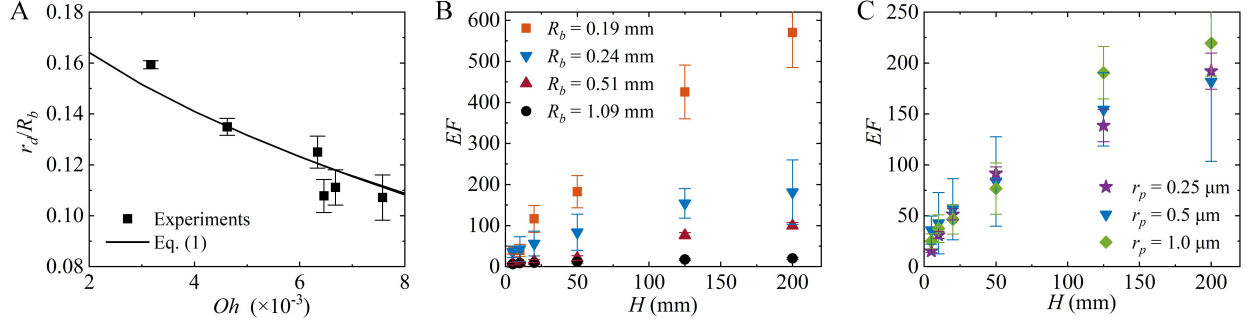


Figure 2: (A) Top jet drop radius r_d scaled by the bubble radius R_b as a function of the Ohnesorge number $Oh(= \mu/\sqrt{\rho_w R_b \gamma})$. Experimental results are captured by Eq. 1.⁴⁸ Error bars represent the standard deviation of data of at least 3 runs. (B) The enrichment factor EF of particles of radius $r_p = 0.5 \mu\text{m}$ in the top jet drop as a function of bubble rising distance H with $R_b = 0.19 - 1.09$ mm. EF increases with increasing H and decreasing R_b . (C) EF of particles in the top jet drop as a function of bubble rising distance H with $r_p = 0.25 - 1 \mu\text{m}$ and $R_b = 0.28 \pm 0.04$ mm, showing EF is independent of r_p in the current experiments. Error bars represent the standard deviation of data of at least 10 runs.

Particle scavenging by bubble rising

The suspended particles are scavenged by the bubble during rising, as illustrated by Figure 3(A), where the particle size is much smaller than the bubble radius ($r_p \ll R_b$). Therefore, the concentration of particles at the rising bubble surface will become enriched compared with that of the bulk water. In the current experiments, considering the small r_p and minor density difference between particle and water, gravitational effects can be ignored.⁴⁹ Meanwhile,

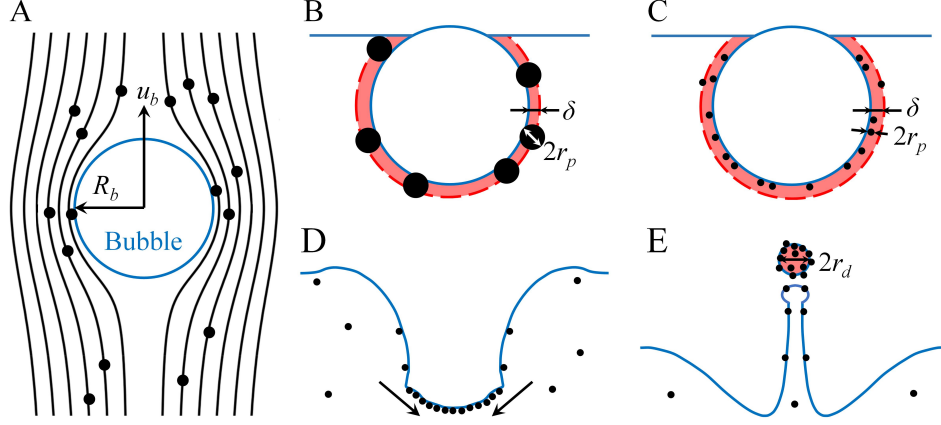


Figure 3: Mechanism of particulate enrichment in bubble bursting jet drop. (A) A rising bubble collects particles from the contaminated water by interception. Small particles with negligible inertia follow the streamlines, with only those close to the bubble surface being intercepted and carried by the bubble. Sketches of a bubble carrying particles at the water surface where (B) the particle diameter $2r_p$ is larger than the thickness of the liquid shell δ forming the top jet drop after bursting (Regime I) or (C) $2r_p < \delta$ (Regime II). (D) During bubble bursting, bubble cavity collapse excites capillary waves propagating along the bubble cavity surface, which sweep the particles towards the bubble bottom pole. (E) A jet then forms and eventually pinches off, ejecting a top jet drop with a enriched particle concentration.

for particles with $r_p > 0.1 \mu\text{m}$, diffusive effects can also be neglected.⁵⁰ Additionally, the Stokes number (comparing the particle response time to the fluid characteristic time scales), $St = (\rho_p - \rho_w)r_p^2 u_b / (9\mu R_b)$ with ρ_p the particle density and u_b the bubble velocity, of the particles in our experiments is $< 10^{-4}$, indicating that the particles can be considered as inertialess, and follow the flow streamlines. Thus, the capture of suspended particles by the rising bubble is dominated by the interception mechanism.^{49,50} Considering the Reynolds number ($Re = 2\rho_w u_b R_b / \mu \approx 20 - 600$, comparing the inertial to viscous effects) of the rising bubbles in our experiments, the flow around the bubble can be well approximated as potential flow, allowing for the neglect of viscous and rotational effects.⁵¹ Given such assumptions, a distance from the bubble center-line under which all particles collide and attached can be derived as $\sqrt{3r_p/R_b}$,^{24,52} which gives the collision efficiency of the particles in the liquid volume ($V_s = \pi R_b^2 H$) swept by the rising bubble, $E_c = 3r_p/R_b$. In our experiments, all bubbles rise in a rectilinear trajectory without significant path instability. In addition, we

assume the small particles are attached to the surface upon collision and the coating does not change the surface mobility significantly. Therefore, the number of particles attached to the rising bubble surface can be calculated as $N_c = E_c V_s C_b = 3\pi R_b r_p H C_b$.

Particle collection during bubble bursting

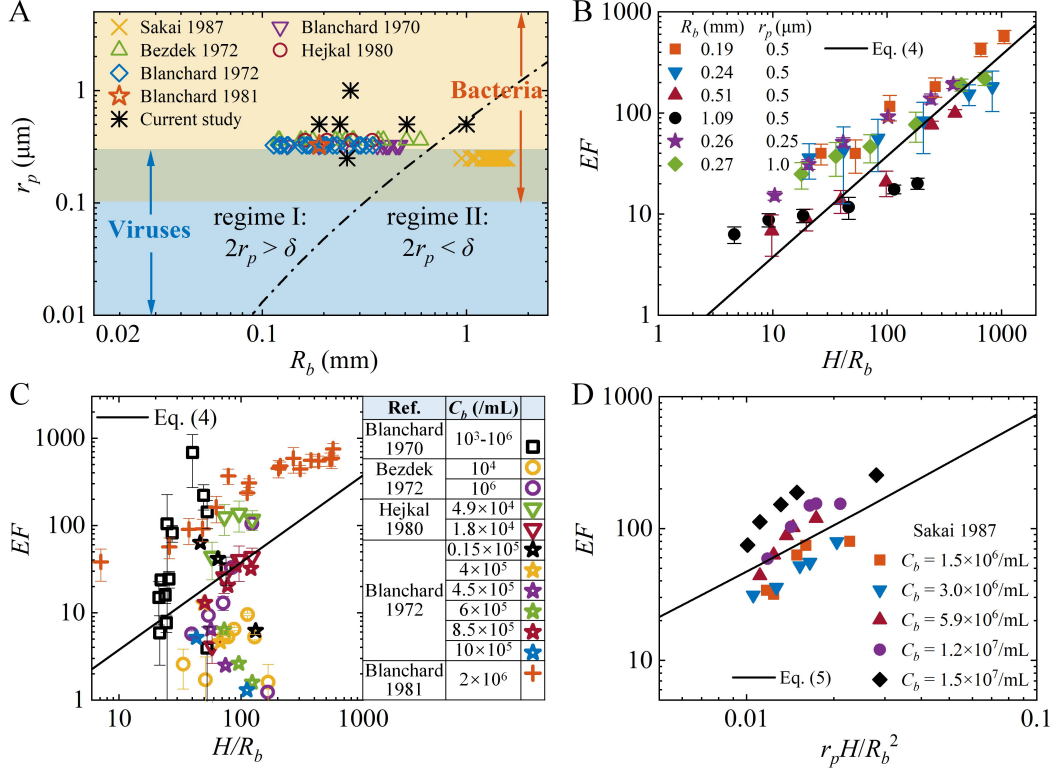


Figure 4: (A) Regime map for cases where $2r_p > \delta$ and $2r_p < \delta$ regarding the bubble radius R_b and particle radius r_p , with the boundary between the two regimes denoted by the dash-dotted line. The parameter range of previous studies^{28,32,40–43} and this study are shown as scatters. The blue and yellow areas represent the size range of viruses and bacteria, respectively. (B) The enrichment factor EF of particles in the top jet drop as a function of the normalized bubble rising distance H/R_b in regime I. Eq. 4 (line) agrees with the experimental results (scatters) well over a wide parameter range. (C) Comparison between the model-predicted EF (Eq. 4, line) and the experimental results (scatters) in previous studies using rod-shaped ($0.25 \mu\text{m}$ radius and $1\text{--}2 \mu\text{m}$ length) and spherical ($0.25\text{--}1.5 \mu\text{m}$ radius) bacteria in regime I, where R_b is calculated using Eq. 1 based on the reported r_d .^{28,40–43} (D) Enrichment factor EF of spherical PS particles in the top jet drop as a function of $r_p H / R_b^2$ in regime II with $r_p = 0.25 \mu\text{m}$ and $H = 100 \text{ mm}$. Eq. 5 (line) predicts the previous experimental results (scatters)³² well with a proportionality coefficient of 8.

After the bubble reaches the water surface along with the captured particles, it eventually bursts and accumulates the particles at the bubble cavity surface into the ejected drop, further increasing the particle concentration compared to that in the bulk water, as illustrated by Figures 3(B-E). Due to the sweep of the capillary waves excited by the cavity collapse, the liquid layer beneath the bubble surface is accumulated at the bottom of the bubble during cavity collapse before being ejected upwards, forming jet drops.^{47,48} Based on this insight, MacIntyre³⁶ first proposed an assumption that the top jet drop originates from the liquid shell just beneath the bubble surface (Figures 3(B-E)). This assumption has been validated by numerical simulations on bubble bursting at surfactant-laden surfaces which illustrated the enrichment of surfactants in the jet drop,^{53–55} and has also been successfully adopted in the theoretical model predicting the *EF* of surface-active compounds.¹⁶ By balancing the top jet drop volume ($V_d = 4\pi r_d^3/3$) and the subsurface liquid shell volume ($V_{ls} = 4\pi R_b^2\delta$), the thickness of the subsurface liquid shell (δ) forming the top jet drop is estimated as

$$\delta = 0.0036(1 - (\frac{Oh}{0.031})^{0.5})^3 R_b. \quad (3)$$

In reality, δ may be comparable to the size of nano/micro-sized particles, resulting in two different modes regarding the collection of surface particles into the top jet drop. When $2r_p > \delta$ (Regime I, Figure 3(B)), a portion of the particles may be left behind in the bulk water due to the small jet drop volume,³⁰ though the particle inertia can be neglected. While for $2r_p < \delta$ (Regime II, Figure 3(C)), a majority of the particles may follow the motion of the subsurface liquid shell and enter the top jet drop.³² Figure 4(A) shows a map of these two regimes separated by the dash-dotted line ($2r_p = \delta$) with respect to r_p and R_b . The size range of viruses ($r \approx 10 - 300$ nm)^{56,57} and bacteria ($r \approx 0.1 - 5$ μ m)⁵⁸ are denoted by the blue and yellow regions, respectively. Bubbles with $R_b < 15$ μ m and $R_b > 2.5$ mm in water cannot produce jet drops due to the inhibitions of viscous and gravity effects, respectively,^{13,46} and thus are not shown on the regime map. Since smaller bubbles are much more prevalent in

natural bodies of water as compared to larger ones,^{5,8} the enrichment of microbes due to bubble bursting jetting may largely occur in regime I. We also summarize the parameter range of the prior studies^{28,32,40–43} and our experiments on the regime map. To our best knowledge, most existing studies (except for the experiments performed by Sakai et al.³²) as well as this study (including a set of data located at the boundary) are situated within regime I. Nonetheless, quantitative modeling of the enrichment effect for the jet drops in both regimes is still lacking, which will be the focus of the following discussion.

Scaling laws for the enrichment factor

We first propose a theoretical argument to predict the enrichment factor EF in regime I. Because the particle diameter $2r_p$ is larger than the thickness δ of the subsurface liquid shell forming the top jet drop, we assume that only a portion $\delta/(2r_p)$ of the particles captured by the bubble will be collected into the top jet drop, i.e., the particle number in the top jet drop $N_d = N_a \delta/(2r_p) = 3\pi R_b H \delta C_b/2$. Then, EF can be obtained as

$$EF = \frac{3H}{8R_b}, \quad (4)$$

which indicates that EF is only determined by the normalized bubble rising distance H/R_b . Specifically, EF increases with the bubble rising distance H and decreases with the bubble radius R_b , while being independent of the particle radius r_p in regime I. Such a scaling law captures the findings of our experiments well (Figures 2(B) and 2(C)). Furthermore, the EF s are collapsed to an approximately linear curve as predicted by Eq. 4 when normalizing H with R_b for different R_b and r_p over a wide parameter range, as shown in Figure 4(B). We also compare our model with experimental data from prior studies^{28,40–43} in Figure 4(C). We note that these previous experiments adopted a relatively complicated biological system to study the enrichment of active rod-shaped (*serratia marcescens*^{28,41,42} or *serratia marnorubra*,^{40,43} 0.25 μm in radius and 1-2 μm in length) or spherical (*micrococcus euryhalis*,⁴⁰ 0.25-1.5 μm in

radius) bacteria. The deviations of reported EF of these bacteria may be attributed to the different bacteria surface properties and metabolites of the bacteria (such as the secretion of biosurfactants which may affect the surface tension of water) caused by varying culture conditions^{37,38} and age,⁴⁰ as well as the active movement of the bacteria.^{59,60} Nevertheless, the overall trend yielded by most of these prior studies follows the prediction of Eq. 4. This comparison with previous work highlights the important role of bubble hydrodynamics in pathogen transmission induced by bubble bursting, and the potential of our model for the prediction of nano/micro-sized organism enrichment in bubble bursting jet drops.

In addition, some prior experimental studies reported that the EF of bacteria decreases rapidly when $R_b < 0.2 - 0.3$ mm, approaching unity when $R_b \approx 0.1$ mm;^{28,43} there were no experimental reports with a smaller R_b due to the limitations of bubble formation. A proposed explanation for this observation is that fewer bacteria are drawn into the jet drop as most bacteria are left behind in the bulk water when the bacteria size is larger than δ .^{23,30} However, our current work demonstrates a continuously increasing particulate EF with decreasing R_b within a wide range of R_b (0.19-1.09 mm) in regime I with $2r_p > \delta$, showing EF can be up to 571 ± 86 for $R_b = 0.19$ mm attributed to the combination effect of bubble scavenge and bursting on the transport of nano/micro-sized particles. Thus, our study may help rule out the effect of bubble hydrodynamics as an explanation for the prior finding of a much smaller EF of bacteria than expected at small R_b . We speculate that the previous experimental observation may originate from the statistics of bacteria sampling and culturing of the jet drops. In these experiments, the average bacteria count in the top jet drop generated by such small bubbles is much less than 1, which may be inadequate for the purpose of sampling.^{43,61} Additionally, the hydrodynamic stresses induced by jet breakup increase exponentially with decreasing jet drop (or bubble) radius.⁶² It is likely that a portion of the bacteria are killed during these experiments with such small bubbles,^{27,63} preventing them from being cultured and thereby causing an underestimate in the original bacteria concentration in the jet drops.

For the particulate enrichment in regime II with $2r_p < \delta$, we assume all the particles captured by the rising bubble are concentrated in the top jet drop, i.e. $N_d = N_a$. Thus, we have

$$EF \sim \frac{423r_p H}{(1 - (Oh/0.031)^{0.5})^3 R_b^2}, \quad (5)$$

which shows that EF is mainly determined by both H/R_b and the particle to bubble radius ratio r_p/R_b , considering the small change of Oh ($= 0.003 - 0.008$) in our experiments. Different from that in regime I, EF is influenced by particle radius r_p , and proportional to R_b^{-2} in regime II. A comparison between the prediction of Eq. 5 and the experimental results of Sakai et al.³² is presented in Figure 4(D). This comparison shows that EF agrees well with Eq. 5 under different bulk particle concentrations, suggesting the validation of our model for the prediction of particulate enrichment in regime II.

It should be noted that the capture of particles by the rising bubble surface may be saturated under high rising distances H and particle concentrations C_b , when the surface concentration of the particles reach a maximum value, and a maximum EF may occur.^{16,42} In this study, we performed experiments at a parameter range without such a particle saturation to identify the effects of the bubble and particle dimensions, as well as the bubble rising distance. The maximum attainable particulate EF in the jet drop and the effects of the related control parameters deserve more attention in future studies. In addition, smaller bubbles with a smaller Re during rising may invalidate the potential flow assumption, necessitating a modification of particle-bubble collision model.⁶⁴ For particulates with $r_p < 0.1 \mu\text{m}$ (such as surfactant molecules¹⁶) or $r_p > 1 \mu\text{m}$ (with a relative large St number), the bubble scavenge may involve diffusive and inertia effects, respectively.^{16,64} Furthermore, microbes in practical situations can exhibit different surface wettabilities or surface charges,^{65,66} which may change the particle attachment as well as the surface mobility of bubbles.²⁴ Considering all these factors could extend our model to a wider parameter range and a more biorelevant dispersal environment in future work.

Conclusion

In summary, we investigate experimentally and theoretically the enrichment of nano/micro-sized particles in bubble bursting jet drops. Via high-speed visualization and direct measurement, we rationalize the detailed mechanism of particulate enrichment, resulting from a two-stage hydrodynamic process: the suspended particles are first intercepted by the rising bubble, attaching to the bubble surface before being skimmed off and concentrated into the jet drop originating from a thin liquid shell beneath the bubble surface during bubble bursting. By modeling the scavenge and collection of particles from the bulk fluid to the jet during bubble rising and bursting, we propose scaling laws for the particle enrichment factor in the top jet drop, which quantitatively agree with our experiments and prior studies³² on the enrichment of spherical particles. Furthermore, the proposed model reasonably captures the overall trend of enrichment factor of active bacteria with a wide range of experimental parameters reported in previous studies,^{28,40–43} thus characterizing the multi-phase fluid dynamics behind the water-to-air transmission of nano/micro-sized organisms via bubble bursting jets.

Regarding the water-to-air disease transmission from toilets,⁶⁷ swimming pools,⁶⁸ tubs,⁶⁹ and wastewater plants,⁷⁰ this study may provide potential guidelines to predict the pathogen load in bubble bursting aerosols and the infection risks resulting from their inhalation,^{71,72} advancing the evaluation and prevention of the indoor and community disease transmission related to bubble bursting.^{34,35} On a planetary scale, modeling the compositions of sea spray aerosol is essential since it dictates the radiant properties of the atmosphere, in addition to impacting atmospheric pollution, global climate, and ecological and material cycles,^{2,27,73–75} with nanoplastics and microplastics found in sea spray aerosols being of major concern in recent years.^{20,21} By advancing the quantification of the particulate concentration in bubble bursting aerosols, our study may be incorporated into a global model for more accurate prediction of sea spray aerosol compositions.

Materials and Methods

Materials

Amino-modified polystyrene (PS) particles (spherical, fluorescent pink, 1.0 wt% aqueous suspension) with a mean radius of $r_p = 0.25 \mu\text{m}$ were purchased from Spherotech, and amino-modified PS particles (spherical, fluorescent orange, 2.5 wt% aqueous suspension) with $r_p = 0.5$ and $1 \mu\text{m}$ were purchased from Sigma-Aldrich. These particle suspensions with $r_p = 0.25, 0.5$ and $1 \mu\text{m}$ were diluted with DI water (resistivity = $18.2 \text{ M}\Omega \text{ cm}$, Smart2Pure 3 UV/UF, Thermo Fisher Scientific) by 64000, 20000, and 2500 times respectively, for a number concentration of $C_b \approx 2.3 \times 10^6/\text{mL}$ used in the experiment. Experiments were performed at $22 \pm 2^\circ\text{C}$ and 1 atm. The surface tensions of the aqueous particle suspensions were measured using the pendant-drop method as $\gamma = 0.073 \text{ N/m}$. In this study, $\rho_w = 998.2 \text{ kg/m}^3$, $\mu = 0.89 \text{ mPa s}$ and $\rho_p = 1050 \text{ kg/m}^3$.

Methods

A square transparent acrylic tank with a cross-sectional area of $30 \times 30 \text{ mm}^2$ was designed to hold the aqueous particle suspensions (Figure 1(A)), which were agitated with a vortex mixer (Thermo Scientific) to ensure homogeneity prior to the conduct of experiments. A micropipette (with tip diameters of 1, 5, and $30 \mu\text{m}$, from Fisher Scientific) or a stainless blunt steel needle (27 Gauge) was used to generate gas bubbles at a depth H beneath the water surface, via a syringe pump (11 Pico Plus Elite, Harvard Apparatus) with a bubbling frequency of < 6 bubbles per minute. The bubble formation in the bulk water (Figure 1(B)) and bursting at the water surface (Figure 1(C)) were visualized by a high-speed camera (FASTCAM Mini AX200, Photron) equipped with focus lens of magnification $3 - 6\times$, illuminated by an LED panel. A frame rate of 6400-20000 frames per second and an exposure time of $5\text{-}50 \mu\text{s}$ were used. The obtained images were further processed using Fiji (ImageJ)⁷⁶ to calculate the bubble radius R_b and the top jet drop radius r_d , which are

confirmed to remain constant during every experiment. A glass slide is placed above the water surface, with the distance between the slide and the water surface being adjusted to ensure that only the top jet drop is collected by the slide, which is confirmed by the high-speed footage (Figure 1(D)). The collected drop is dried before being examined under a microscope (Nikon ECLIPSE Ti2, Nikon) with an objective lens of 10X, 20X or 40X, and the the number of particles in the entire jet drop (N_d) is determined via an in-house image analysis code using MATLAB 2021a (Figure 1(E)). Similarly, a pipette is used to collect a drop from the bulk suspension, with the drop volume (V_b) being verified via the high-speed camera before being dried on a glass slide and examined under the microscope (Figure 1(F)), the same MATLAB image analysis code is used to determine the number of particles in the entire bulk drop (N_b). In every experiment, at least 10 top jet drops and 3 bulk drops are examined to determine the average N_d and N_b , respectively.

Acknowledgement

This work is partially supported by American Chemical Society Petroleum Research Fund Grant No. 61574-DNI9 (to J.F.)

Supporting Information Available

The Supporting Information is available free of charge on the ACS Publications website at XXX

Video of bubble formation from a micropipette (AVI)

Video of bubble bursting at the surface of particle suspension (AVI)

Video of the collection of the top jet drop by a glass slide (AVI)

References

- (1) Knelman, F.; Dombrowski, N.; Newitt, D. Mechanism of the bursting of bubbles. *Nature* **1954**, *173*, 261–261.
- (2) Deike, L. Mass transfer at the ocean–atmosphere interface: The role of wave breaking, droplets, and bubbles. *Annu. Rev. Fluid Mech.* **2022**, *54*, 191–224.
- (3) Lewis, E. R.; Lewis, E. R.; Lewis, R.; Karlstrom, K. E.; Schwartz, S. E. *Sea salt aerosol production: mechanisms, methods, measurements, and models*; American geophysical union: Washington, DC, 2004; Vol. 152.
- (4) Jiang, X.; Rotily, L.; Villiermaux, E.; Wang, X. Submicron drops from flapping bursting bubbles. *Proceedings of the National Academy of Sciences* **2022**, *119*.
- (5) Deane, G. B.; Stokes, M. D. Scale dependence of bubble creation mechanisms in breaking waves. *Nature* **2002**, *418*, 839–844.
- (6) Edzwald, J. K. Principles and applications of dissolved air flotation. *Water Sci. Technol.* **1995**, *31*, 1–23.
- (7) Cartmill, J. W.; Su, M. Y. Bubble size distribution under saltwater and freshwater breaking waves. *Dyn. Atmospheres Oceans* **1993**, *20*, 25–31.
- (8) Blenkinsopp, C. E.; Chaplin, J. R. Bubble size measurements in breaking waves using optical fiber phase detection probes. *IEEE J. Ocean. Eng* **2010**, *35*, 388–401.
- (9) Brasz, C. F.; Bartlett, C. T.; Walls, P. L.; Flynn, E. G.; Yu, Y. E.; Bird, J. C. Minimum size for the top jet drop from a bursting bubble. *Phys. Rev. Fluids* **2018**, *3*, 074001.
- (10) Blanco-Rodríguez, F. J.; Gordillo, J. On the sea spray aerosol originated from bubble bursting jets. *J. Fluid Mech.* **2020**, *886*.

- (11) Berny, A.; Popinet, S.; Séon, T.; Deike, L. Statistics of jet drop production. *Geophys. Res. Lett.* **2021**, *48*, e2021GL092919.
- (12) Gañán-Calvo, A. M.; López-Herrera, J. M. On the physics of transient ejection from bubble bursting. *J. Fluid Mech.* **2021**, *929*.
- (13) Veron, F. Ocean spray. *Annu. Rev. Fluid Mech.* **2015**, *47*, 507–538.
- (14) Wang, X.; Deane, G. B.; Moore, K. A.; Ryder, O. S.; Stokes, M. D.; Beall, C. M.; Collins, D. B.; Santander, M. V.; Burrows, S. M.; Sultana, C. M., et al. The role of jet and film drops in controlling the mixing state of submicron sea spray aerosol particles. *Proceedings of the National Academy of Sciences* **2017**, *114*, 6978–6983.
- (15) O’Dowd, C. D.; Smith, M. H.; Consterdine, I. E.; Lowe, J. A. Marine aerosol, sea-salt, and the marine sulphur cycle: A short review. *Atmos. Environ.* **1997**, *31*, 73–80.
- (16) Chingin, K.; Yan, R.; Zhong, D.; Chen, H. Enrichment of surface-active compounds in bursting bubble aerosols. *ACS Omega* **2018**, *3*, 8709–8717.
- (17) O’Dowd, C. D.; Facchini, M. C.; Cavalli, F.; Ceburnis, D.; Mircea, M.; Decesari, S.; Fuzzi, S.; Yoon, Y. J.; Putaud, J.-P. Biogenically driven organic contribution to marine aerosol. *Nature* **2004**, *431*, 676–680.
- (18) Ji, B.; Yang, Z.; Feng, J. Compound jetting from bubble bursting at an air-oil-water interface. *Nat. Commun.* **2021**, *12*, 1–10.
- (19) Sampath, K.; Afshar-Mohajer, N.; Chandrala, L. D.; Heo, W.-S.; Gilbert, J.; Austin, D.; Koehler, K.; Katz, J. Aerosolization of crude oil-dispersant slicks due to bubble bursting. *J. Geophys. Res. Atmos.* **2019**, *124*, 5555–5578.
- (20) Masry, M.; Rossignol, S.; Roussel, B. T.; Bourgogne, D.; Bussi re, P.-O.; R’mili, B.; Wong-Wah-Chung, P. Experimental evidence of plastic particles transfer at the water-air interface through bubble bursting. *Environ. Pollut.* **2021**, *280*, 116949.

- (21) Allen, S.; Allen, D.; Moss, K.; Le Roux, G.; Phoenix, V. R.; Sonke, J. E. Examination of the ocean as a source for atmospheric microplastics. *PLOS One* **2020**, *15*, e0232746.
- (22) Baylor, E. R.; Peters, V.; Baylor, M. B. Water-to-air transfer of virus. *Science* **1977**, *197*, 763–764.
- (23) Blanchard, D. C. *Air-sea exchange of gases and particles*; Springer, 1983; pp 407–454.
- (24) Walls, P. L.; Bird, J. C.; Bourouiba, L. Moving with bubbles: a review of the interactions between bubbles and the microorganisms that surround them. *Am. Zool.* **2014**, *54*, 1014–1025.
- (25) Séon, T.; Liger-Belair, G. Effervescence in champagne and sparkling wines: From bubble bursting to droplet evaporation. *Eur. Phys. J.: Spec. Top.* **2017**, *226*, 117–156.
- (26) Spiel, D. E. On the births of jet drops from bubbles bursting on water surfaces. *J. Geophys. Res. Oceans* **1995**, *100*, 4995–5006.
- (27) Hariadi, R. F.; Winfree, E.; Yurke, B. Determining hydrodynamic forces in bursting bubbles using DNA nanotube mechanics. *Proceedings of the National Academy of Sciences* **2015**, *112*, E6086–E6095.
- (28) Blanchard, D. C.; Syzdek, L. Mechanism for the water-to-air transfer and concentration of bacteria. *Science* **1970**, *170*, 626–628.
- (29) Joung, Y. S.; Ge, Z.; Buie, C. R. Bioaerosol generation by raindrops on soil. *Nat. Commun.* **2017**, *8*, 1–10.
- (30) Blanchard, D. C. The ejection of drops from the sea and their enrichment with bacteria and other materials: a review. *Estuaries* **1989**, *12*, 127–137.
- (31) Burrows, S. M.; Ogunro, O.; Frossard, A.; Russell, L. M.; Rasch, P. J.; Elliott, S. A physically based framework for modeling the organic fractionation of sea spray aerosol

- from bubble film Langmuir equilibria. *Atmospheric Chem. Phys.* **2014**, *14*, 13601–13629.
- (32) Sakai, M.; Tanaka, A.; Egawa, H.; Sugihara, G. Enrichment of suspended particles in top jet drops from bursting bubbles. *J. Colloid Interface Sci.* **1988**, *125*, 428–436.
- (33) Sakai, M. Ion distribution at a nonequilibrium gas/liquid interface. *J. Colloid Interface Sci.* **1989**, *127*, 156–166.
- (34) Bourouiba, L. The fluid dynamics of disease transmission. *Annu. Rev. Fluid Mech.* **2020**, *53*.
- (35) Lou, M.; Liu, S.; Gu, C.; Hu, H.; Tang, Z.; Zhang, Y.; Xu, C.; Li, F. The bioaerosols emitted from toilet and wastewater treatment plant: a literature review. *Environ. Sci. Pollut. Res.* **2021**, *28*, 2509–2521.
- (36) MacIntyre, F. Flow patterns in breaking bubbles. *J. Geophys. Res.* **1972**, *77*, 5211–5228.
- (37) Syzdek, L. D. Influence of *Serratia marcescens* pigmentation on cell concentrations in aerosols produced by bursting bubbles. *Appl. Environ. Microbiol.* **1985**, *49*, 173–178.
- (38) Burger, S. R.; Bennett, J. Droplet enrichment factors of pigmented and nonpigmented *Serratia marcescens*: possible selective function for prodigiosin. *Appl. Environ. Microbiol.* **1985**, *50*, 487–490.
- (39) Sakai, M.; Kuroda, M.; Matsumoto, M.; Kusunoki, K. *Biochemical Engineering for 2001*; Springer, 1992; pp 537–539.
- (40) Hejkal, T.; LaRock, P.; Winchester, J. Water-to-air fractionation of bacteria. *Appl. Environ. Microbiol.* **1980**, *39*, 335–338.
- (41) Blanchard, D. C.; Syzdek, L. D. Concentration of bacteria in jet drops from bursting bubbles. *J. Geophys. Res.* **1972**, *77*, 5087–5099.

- (42) Blanchard, D. C.; Syzdek, L. D.; Weber, M. E. Bubble scavenging of bacteria in fresh-water quickly produces bacterial enrichment in airborne jet drops 1. *Limnol. Oceanogr.* **1981**, *26*, 961–964.
- (43) Bezdek, H.; Carlucci, A. SURFACE CONCENTRATION OF MARINE BACTERIA 1. *Limnol. Oceanogr.* **1972**, *17*, 566–569.
- (44) Blanchard, D. C.; Syzdek, L. D. Seven problems in bubble and jet drop researches 1. *Limnol. Oceanogr.* **1978**, *23*, 389–400.
- (45) Gañán-Calvo, A. M. Revision of bubble bursting: Universal scaling laws of top jet drop size and speed. *Phys. Rev. Lett.* **2017**, *119*, 204502.
- (46) Walls, P. L.; Henaux, L.; Bird, J. C. Jet drops from bursting bubbles: How gravity and viscosity couple to inhibit droplet production. *Phys. Rev. E* **2015**, *92*, 021002.
- (47) Gordillo, J.; Rodríguez-Rodríguez, J. Capillary waves control the ejection of bubble bursting jets. *J. Fluid Mech.* **2019**, *867*, 556–571.
- (48) Blanco-Rodríguez, F. J.; Gordillo, J. On the jets produced by drops impacting a deep liquid pool and by bursting bubbles. *J. Fluid Mech.* **2021**, *916*.
- (49) Weber, M. E.; Blanchard, D. C.; Syzdek, L. D. The mechanism of scavenging of water-borne bacteria by a rising bubble. *Limnol. Oceanogr.* **1983**, *28*, 101–105.
- (50) Walls, P. L.; Bird, J. C. Enriching particles on a bubble through drainage: Measuring and modeling the concentration of microbial particles in a bubble film at rupture. *Elementa (Wash. D C)* **2017**, *5*.
- (51) Manica, R.; Klaseboer, E.; Chan, D. Y. The hydrodynamics of bubble rise and impact with solid surfaces. *Adv. Colloid Interface Sci.* **2016**, *235*, 214–232.
- (52) Sutherland, K. Physical chemistry of flotation. XI. Kinetics of the flotation process. *J. Phys. Chem.* **1948**, *52*, 394–425.

- (53) Constante-Amores, C. R.; Kahouadji, L.; Batchvarov, A.; Shin, S.; Chergui, J.; Juric, D.; Matar, O. K. Dynamics of a surfactant-laden bubble bursting through an interface. *J. Fluid Mech.* **2021**, *911*.
- (54) Boulton-Stone, J. M. The effect of surfactant on bursting gas bubbles. *J. Fluid Mech.* **1995**, *302*, 231–257.
- (55) Dey, D.; Boulton-Stone, J.; Emery, A.; Blake, J. Experimental comparisons with a numerical model of surfactant effects on the burst of a single bubble. *Chem. Eng. Sci.* **1997**, *52*, 2769–2783.
- (56) Louten, J. Virus structure and classification. *Essential Human Virology* **2016**, 19.
- (57) Colson, P.; La Scola, B.; Levasseur, A.; Caetano-Anollés, G.; Raoult, D. Mimivirus: leading the way in the discovery of giant viruses of amoebae. *Nat. Rev. Microbiol.* **2017**, *15*, 243–254.
- (58) Levin, P. A.; Angert, E. R. Small but mighty: cell size and bacteria. *Cold Spring Harb. Perspect. Biol.* **2015**, *7*, a019216.
- (59) Lushi, E.; Wioland, H.; Goldstein, R. E. Fluid flows created by swimming bacteria drive self-organization in confined suspensions. *Proceedings of the National Academy of Sciences* **2014**, *111*, 9733–9738.
- (60) Zhang, H. P.; Be’er, A.; Florin, E.-L.; Swinney, H. L. Collective motion and density fluctuations in bacterial colonies. *Proceedings of the National Academy of Sciences* **2010**, *107*, 13626–13630.
- (61) Quinn, J. A.; Steinbrook, R. A.; Anderson, J. L. Breaking bubbles and the water-to-air transport of particulate matter. *Chem. Eng. Sci.* **1975**, *30*, 1177–1184.
- (62) McRae, O.; Mead, K. R.; Bird, J. C. Aerosol agitation: quantifying the hydrodynamic

- stressors on particulates encapsulated in small droplets. *Phys. Rev. Fluids* **2021**, *6*, L031601.
- (63) Walls, P. L.; McRae, O.; Natarajan, V.; Johnson, C.; Antoniou, C.; Bird, J. C. Quantifying the potential for bursting bubbles to damage suspended cells. *Sci. Rep.* **2017**, *7*, 1–9.
- (64) Dai, Z.; Fornasiero, D.; Ralston, J. Particle–bubble collision models—a review. *Adv. Colloid Interface Sci.* **2000**, *85*, 231–256.
- (65) van der Wal, A.; Norde, W.; Zehnder, A. J.; Lyklema, J. Determination of the total charge in the cell walls of Gram-positive bacteria. *Colloids Surf. B: Biointerfaces* **1997**, *9*, 81–100.
- (66) Gannon, J.; Manilal, V.; Alexander, M. Relationship between cell surface properties and transport of bacteria through soil. *Appl. Environ. Microbiol.* **1991**, *57*, 190–193.
- (67) Abney, S.; Bright, K.; McKinney, J.; Ijaz, M. K.; Gerba, C. Toilet hygiene—review and research needs. *J. Appl. Microbiol.* **2021**, *131*, 2705–2714.
- (68) Angenent, L. T.; Kelley, S. T.; Amand, A. S.; Pace, N. R.; Hernandez, M. T. Molecular identification of potential pathogens in water and air of a hospital therapy pool. *Proceedings of the National Academy of Sciences* **2005**, *102*, 4860–4865.
- (69) Embil, J.; Warren, P.; Yakrus, M.; Stark, R.; Hershfield, E. Pulmonary illness associated with exposure to Mycobacterium-avium complex in hot tub water. Hypersensitivity pneumonitis or infection? *Chest* **1997**, *111*, 813–816.
- (70) Bauer, H.; Fuerhacker, M.; Zibuschka, F.; Schmid, H.; Puxbaum, H. Bacteria and fungi in aerosols generated by two different types of wastewater treatment plants. *Water Res.* **2002**, *36*, 3965–3970.

- (71) Azimi, P.; Keshavarz, Z.; Laurent, J. G. C.; Stephens, B.; Allen, J. G. Mechanistic transmission modeling of COVID-19 on the Diamond Princess cruise ship demonstrates the importance of aerosol transmission. *Proceedings of the National Academy of Sciences* **2021**, *118*.
- (72) Lelieveld, J.; Helleis, F.; Borrmann, S.; Cheng, Y.; Drewnick, F.; Haug, G.; Klimach, T.; Sciare, J.; Su, H.; Pöschl, U. Model calculations of aerosol transmission and infection risk of COVID-19 in indoor environments. *Int. J. Environ. Res. Public Health* **2020**, *17*, 8114.
- (73) Brooks, S. D.; Thornton, D. C. Marine Aerosols and Clouds. *Annu. Rev. Mar. Sci.* **2018**, *10*, 289–313.
- (74) Schiffer, J. M.; Mael, L. E.; Prather, K. A.; Amaro, R. E.; Grassian, V. H. Sea Spray Aerosol: Where Marine Biology Meets Atmospheric Chemistry. *ACS Cent. Sci.* **2018**, *4*.
- (75) O’Dowd, C. D.; Smith, M. H.; Consterdine, I. E.; Lowe, J. A. Marine aerosol, sea-salt, and the marine sulphur cycle: a short review. *Atmos. Environ.* **1997**, *31*, 73–80.
- (76) Schindelin, J.; Arganda-Carreras, I.; Frise, E.; Kaynig, V.; Longair, M.; Pietzsch, T.; Preibisch, S.; Rueden, C.; Saalfeld, S.; Schmid, B., et al. Fiji: an open-source platform for biological-image analysis. *Nat. methods* **2012**, *9*, 676–682.

Graphical TOC Entry

